

Classification and visualization of primary trabecular bone in lumbar vertebrae

Khairul Salleh Basaruddin^{*1}, Junya Omori², Naoki Takano³ and Takayoshi Nakano⁴

¹School of Mechatronic Engineering, Universiti Malaysia Perlis, 02600 Pauh Putra, Perlis, Malaysia

²Graduate School of Science and Technology, Keio University, 3-14-1 Hiyoshi, Yokohama, 223-8522, Japan

³Department of Mechanical Engineering, Keio University, 3-14-1 Hiyoshi, Yokohama, 223-8522, Japan

⁴Division of Materials and Manufacturing Science, Osaka University, 2-1, Suita, Osaka 565-0871, Japan

(Received September 11, 2013, Revised January 19, 2014, Accepted May 14, 2014)

Abstract. The microarchitecture of trabecular bone plays a significant role in mechanical strength due to its load-bearing capability. However, the complexity of trabecular microarchitecture hinders the evaluation of its morphological characteristics. We therefore propose a new classification method based on static multiscale theory and dynamic finite element method (FEM) analysis to visualize a three-dimensional (3D) trabecular network for investigating the influence of trabecular microarchitecture on load-bearing capability. This method is applied to human vertebral trabecular bone images obtained by micro-computed tomography (micro-CT) through which primary trabecular bone is successfully visualized and extracted from a highly complicated microarchitecture. The morphological features were then analyzed by viewing the percolation of load pathways in the primary trabecular bone by using the stress wave propagation method analyzed under impact loading. We demonstrate that the present method is effective for describing the morphology of trabecular bone and has the potential for morphometric measurement applications.

Keywords: vertebra; trabecular network; morphology; image-based modeling; homogenization method; dynamic FEM

1. Introduction

It is widely accepted that the mechanical properties of trabecular bone should be characterized by both bone density and bone quality. Although there are many descriptions of bone quality have been reported (Nakano *et al.* 2002, Basaruddin *et al.* 2013), the present study focuses on the morphology of the trabecular network architecture of human lumbar vertebra. It has been reported that the connectivity (Kinney and Ladd 1998) and morphology characteristics (Shi *et al.* 2009) contribute to the effectiveness of load-bearing distribution. The primary trabecular bone in the fourth lumbar vertebra (L4) is aligned to support mainly self-weight in the vertical direction. Due to its complexity, however, the architecture of this bone has not been clarified thus far.

Recent advancement of three-dimensional (3D) imaging techniques allow for realistic reconstruction of trabecular microarchitecture based on an actual bone specimen. However,

*Corresponding author, Ph.D., E-mail: khsalleh@unimap.edu.my

challenges remain in obtaining the morphological and topological characterizations from trabecular microstructures because a local view of the trabecular network is needed to provide information on the microarchitecture. Several computational techniques are available for this task (Lee *et al.* 2006, Andrade Silva *et al.* 2010), including the use of 3D skeleton graph analysis (Stauber and Müller 2006, Liu *et al.* 2008). This method, initially introduced to characterize granular porous media in sedimentary rock (Lin and Cohen 1982), has been recently applied to study trabecular bone microarchitecture and enables its full decomposition into individual trabecular rods and plates. Moreover, the 3D skeletonization technique provides a local characterization on the morphology and orientation of trabecular bone. A correlation between trabecular morphology and apparent mechanical properties has been commonly described by morphometric parameters (Stauber and Müller 2006, Liu *et al.* 2009) benefited from this technique. For example, the line skeleton graph analysis (LSGA) method was introduced to compute topological parameters, including the length and volume of a single trabecula (Pothaud *et al.* 2000). This method shows the effect of individual trabecular scales to mechanical properties. Moreover, Saha *et al.* (2000) developed digital topological analysis (DTA) for the characterization of trabecular architecture by subdividing trabeculae plates and rods on the basis of the skeletonization technique. They showed that locally determined orientations can describe the anisotropy of a trabecular network better than the mean intercept length (MIL) parameter. More recently, the trabecular microstructure has successfully been decomposed volumetrically into its basic elements of plates and rods (Stauber and Müller 2006, Liu *et al.* 2008) to investigate the influence of morphology via morphometric parameters on the mechanical stiffness of trabecular bone. However, discussions on the influence of the trabecular network architecture on the load distribution in the entire vertebral column are relatively scarce.

One of the authors of this paper has previously reported that the principal stress vector display is useful for visualizing the mechanical load pathways in peri-implant trabecular bone (Ohashi *et al.* 2010). Although the principal stress contour display can also highlight the primary bone in human vertebral trabecular bone (Tawara *et al.* 2008), the following two issues remain unresolved. The principal stress contour display determined by static analysis is useful for only very small regions, such as a 2.1 mm cubic area, and is obviously insufficient for explaining the trabecular network system in human vertebrae. The second problem is that the color scale must be adjusted, and there is no known systematic method for determining the stress threshold for display. The stress wave, however, propagates into all branches in the network system. To eliminate such branches without percolation, static FEM is used prior to that of dynamic FEM. To define the stress threshold used to classify the primary trabecular bone in vertebrae, the averaging principle used in the asymptotic homogenization method (Guedes and Kikuchi 1990) is employed in the present study. The outline of the static homogenization theory is described in section 3.1, and its reliability has been demonstrated by comparison with experimental measurements conducted for engineering materials (Takano *et al.* 2003, Takano *et al.* 2010).

Dynamic FEM analysis and impact analysis are frequently used for engineering applications such as automobile crashes. However, dynamic analysis used for infinite solid models may cause problems in transient wave propagation (Kuhlemeyer and Lysmer 1973). The same is true for a small model extracted from large-sized objects. Lysmer and Kuhlemeyer (1969) introduced a special viscous boundary condition for solving this problem, which is employed in the present study as described in section 3.3. Micro-computed tomography (micro-CT) image-based FEM analysis has been recently applied to trabecular bone; however, such research is limited to static analysis. In the dynamic analysis of trabecular bone with image-based modeling, significant

challenges remain in postprocess visualization. Because these large-scale problems require huge amounts of output data, the user must limit the physical quantities for output prior to the analysis. Although this limitation does not affect engineering problems because the location of interest is roughly estimated theoretically prior to the analysis, effective biomechanical analysis of trabecular bone requires numerous output quantities. 3D display is determined to be more useful than cross-sectional display for explaining the network architecture.

Therefore, the purpose of the present study is to visualize the characteristics of primary trabecular bones to provide an understanding of the mechanical role of the highly complicated trabecular network architecture. A new classification and visualization method is used and applied to osteoporotic and healthy human vertebral trabecular bones to display stress wave propagation obtained by dynamic finite element method. Although the microstructure reconstructed from high-resolution micro-CT is highly complicated, the proposed method can be used to enhance the visibility of the trabecular network for large-sized regions, particularly when the role of trabecular morphology on mechanical load transfer is of interest. In contrast to the existing studies (Pothuaud *et al.* 2000, Stauber and Müller 2006, Liu *et al.* 2008), our method proposes the extraction of the trabecular region into percolated portions rather than that into individual rods and plates to enable analysis of the morphology from the perspective of load distribution.

2. Materials

Two trabecular bone samples were extracted from the central part of a human fourth lumbar vertebra (L4). One sample was obtained from an 86-year-old female osteoporotic patient, and the other was taken from healthy bone of a 68-year-old male. The samples were imaged by a micro-CT device (SMX-100CT, Shimadzu, Japan) with 40 kV of voltage and 30 μ A of current. The image resolution was 29.92 μ m for the osteoporotic bone and 31.91 μ m for the healthy bone. The analysis of these bone samples has been approved by an ethics committee.

A binarization technique was applied to convert the 256 gray levels of the micro-CT image into a 3D binary image. The 3D binarized image was obtained by matching the architecture of the micro-CT image with specific portions of the actual bone slices. 3D voxel finite element (FE) models were automatically generated from a sequence of binary images with the same slice distance through image resolution by using eight-node voxel element conversion (Hollister *et al.* 1994). A specific region of interest (ROI) was extracted from each voxel FE model; the specifications are listed in Table 1. Both ROIs are shown in Fig. 1. In this paper, the left–right axis is defined as axis-1, the anterior–posterior axis is axis-2, and the vertical axis is axis-3. ROIs were carefully selected by ensuring the fluctuation of bone volume fraction along the cross-section and at the boundary is almost constant in order to maintain the periodicity of the homogenization

Table 1 Specifications of regions of interest (ROIs)

	Osteoporotic trabecular bone	Healthy trabecular bone
ROI size (mm ³)	5×6.6×12	6×6×12
Element size (μ m ³)	30×30×30	32×32×32
No. of elements	877,277	2,781,416
Bone volume fraction, BV/TV	0.060	0.172

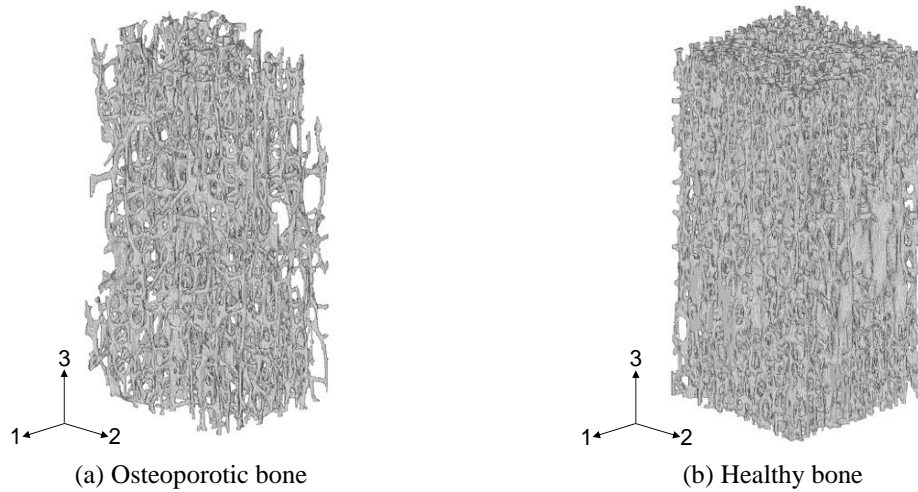


Fig. 1 ROI for osteoporotic and healthy vertebral trabecular bones.

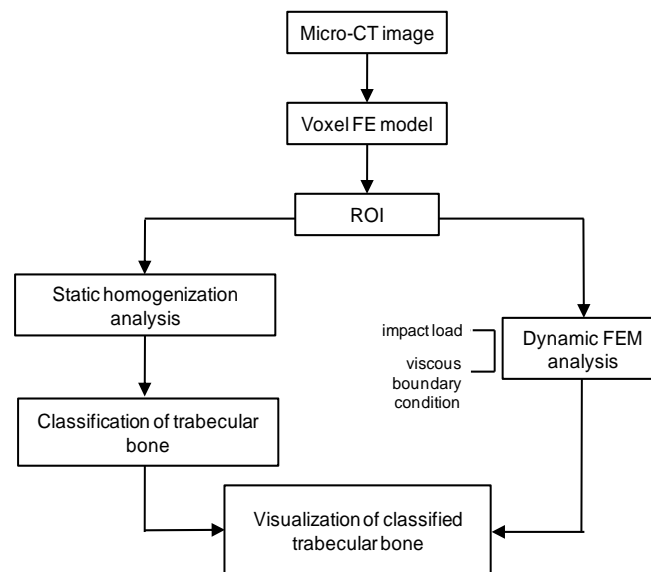


Fig. 2 Hierarchical approach for classification and visualization of trabecular bone.

analysis (Tawara *et al.* 2010). Since the homogenization procedure is to solve a scale-free problem theoretically, and also because as large ROI (or microstructure model) as possible should be used to investigate the load path at microscale, the models in Fig. 1 are used with periodic boundary conditions. The mechanical properties of the trabecular bone tissue were assumed to be linear isotropic with Young's modulus of 10 GPa (Rho *et al.* 1993). Poisson's ratio was set to 0.4 by reference to Keyak *et al.* (1990), Reilly and Burstein (1975) and Van Buskirk and Ashman (1981).

3. Methods

Fig. 2 shows a schematic flowchart of the proposed approach for the classification and visualization of complex trabecular morphology. Once the 3D voxel models are created and ROIs are selected, static homogenization and dynamic analyses are performed separately for the same ROIs. In the static homogenization analysis, the characteristic displacements were obtained. Periodic boundary conditions with respect to the characteristic displacements in three directions were applied to all boundary surfaces (i.e., top, bottom and side surfaces). The FE models used for the present homogenization analysis at the microscale are shown in Fig. 1. Homogenization analysis is applied to classify the trabecular bone into strut elements having significant contribution to the mechanical load transfer. Mechanical stress percolation is visualized through dynamic FEM analysis with focus on the primary trabecular bone in human vertebra. Although stress waves produced by the impact load propagate into the strut elements without percolation, the stress in the static analysis of those particular strut elements is low. Therefore, such strut elements can be eliminated in the classification process to improve the visibility of stress wave propagation in the percolated elements. In the following sections, the outline of static homogenization theory, classification method, and visualization of stress wave propagation by using dynamic FEM analysis are described.

3.1 Outline of static homogenization theory

In the present study, a linearly elastic problem is considered. Because the selected large-sized ROI could represent a trabecular bone region in one lumbar vertebra, the asymptotic homogenization method was applied, which has been the most successful method used for such multiscale computation. For the homogenization to obtain the macroscopic properties, there are some other techniques including the continuum micromechanics. However, more focus is put on the localization process that is to calculate the microscopic stress with rigorously satisfying the averaging principle in this paper. Hence, the asymptotic homogenization method was chosen instead of other micromechanics methods. This technique has been widely used in the analysis of cortical (Parnell *et al.* 2006, Grimal *et al.* 2011) and trabecular bones (Hollister *et al.* 1991, Basaruddin 2013, Matsunaga *et al.* 2013); hence, only the outline of this theory is described here.

At the macroscopic scale x , a macroscopic structure Ω of trabecular bone is expected to have microscopic heterogeneity. Considering the traction force t is applied on the smooth boundary Γ , the macroscopic equation, neglecting the body force, is derived as

$$\int_{\Omega} \mathbf{D}_{ijpq}^H \frac{\partial \mathbf{u}_p^0}{\partial \mathbf{x}_q} \frac{\partial \delta \mathbf{u}_i^0}{\partial \mathbf{x}_j} \mathbf{d}\Omega = \int_{\Gamma} \mathbf{t}_i \delta \mathbf{u}_i^0 \mathbf{d}\Gamma \quad \forall \delta \mathbf{u}_i^0 \quad (1)$$

where u^0 is a macroscopic displacement and D^H is the homogenized elasticity tensor. When a ROI Y representing the global heterogeneity is defined, D^H can be obtained as the volumetric average of the microscopic properties in the ROI, as calculated in Eq. (2).

$$\mathbf{D}_{ijpq}^H = \frac{1}{|Y|} \int_Y \left(\mathbf{D}_{ijpq} - \mathbf{D}_{ijrs} \frac{\partial \chi_r^{pq}}{\partial \mathbf{y}_s} \right) \quad (2)$$

where D is the elasticity tensor of bone, $|Y|$ is the volume of ROI, and χ is a characteristic displacement that is a periodic function with respect to the microscopic scale y . χ is obtained by solving the microscopic equation for ROI Y under the periodic boundary condition as

$$\int_{\mathbf{Y}} \mathbf{D}_{ijrs} \frac{\partial \chi_r^{pq}}{\partial y_s} \frac{\partial \delta \mathbf{u}_i^1}{\partial y_j} d\mathbf{Y} = \int_{\mathbf{Y}} \mathbf{D}_{ijpq} \frac{\partial \delta \mathbf{u}_i^1}{\partial y_j} d\mathbf{Y} \quad \forall \delta \mathbf{u}_i^1 \quad (3)$$

where u^1 represents a perturbed displacement term in the asymptotic expansion method due to the microscopic heterogeneity. Next, the microscopic stress σ subject to either the macroscopic strain E or macroscopic stress $\langle \sigma \rangle$ can be calculated as derived in Eq. (4).

$$\begin{aligned} \sigma_{ij} &= \left(D_{ijpq} - D_{ijrs} \frac{\partial \chi_r^{pq}}{\partial y_s} \right) E_{pq} \\ &= \left(D_{ijpq} - D_{ijrs} \frac{\partial \chi_r^{pq}}{\partial y_s} \right) (D_{pqkl}^H)^{-1} \langle \sigma \rangle_{kl} \end{aligned} \quad (4)$$

Finally, generalization of this multiscale theory can be written in Eq. (5), which assures consistency between the microscopic and macroscopic behaviors of the trabecular bone model.

$$\langle \sigma \rangle = \langle \sigma \rangle = \langle D \rangle \langle \varepsilon \rangle = D^H \cdot E \quad (5)$$

where $\langle \cdot \rangle$ indicates the volumetric averaging operator and ε is microscopic strain.

3.2 Classification of trabecular bone

The procedures used in static homogenization analysis and for the classification of trabecular bone given in Fig. 2 are summarized in Fig. 3. This method consists of the following 10 steps:

1) Select a large ROI $/Y/$ with $X_{ROI} \times Y_{ROI} \times Z_{ROI}$ dimensions, as shown in Fig. 4. Let the coordinate of each element in the ROI be written as in the following Eq. (6).

$$(x, y, z) \in Y \equiv \left(\left[-\frac{X_{ROI}}{2}, \frac{X_{ROI}}{2} \right], \left[-\frac{Y_{ROI}}{2}, \frac{Y_{ROI}}{2} \right], \left[-\frac{Z_{ROI}}{2}, \frac{Z_{ROI}}{2} \right] \right) \quad (6)$$

The ROI has N number of elements with volume $/Y/$.

2) Apply uniform and uniaxial compressive macroscopic stresses sequentially to the selected ROI in orthogonal directions, as shown in Fig. 4, which are indicated as $\langle \sigma \rangle_{11} = -1$, $\langle \sigma \rangle_{22} = -1$, and $\langle \sigma \rangle_{33} = -1$. Axes-1 and 2 correspond to the lateral axes of left–right and posterior–anterior, respectively, whereas axis-3 relates to the vertical axis.

3) Calculate the minimum principal stress response for each voxel element i under three load cases and define them as $(\sigma_3^{(1)})_i$, $(\sigma_3^{(2)})_i$ and $(\sigma_3^{(33)})_i$. The superscript denotes the loading direction.

4) Define the inner part of the ROI and apply the following classification procedure because numerical error may occur in the boundary region of the ROI. The coordinate for the selected inner ROI Y_{in} is written as Eq. (7), following the authors' previous paper (Takano *et al.* 2003), with N_{in} number of elements.

$$Y_{in} \equiv \left(\left[-0.4X_{ROI}, 0.4X_{ROI} \right], \left[-0.4Y_{ROI}, 0.4Y_{ROI} \right], \left[-0.4Z_{ROI}, 0.4Z_{ROI} \right] \right) \quad (7)$$

The volume of the inner ROI can then be calculated as

$$|Y_{in}| = (0.8)^3 |Y| = 0.512 |Y| \quad (8)$$

5) Select the elements located in the inner region, as expressed in Eq. (9); those outside of the inner region are categorized as boundary trabeculae.

$$(x, y, z) \in |Y_{in}| \quad (j = 1, \dots, N) \quad (9)$$

6) Under the vertical load condition, $\langle \sigma \rangle_{33} = -1$, select elements j (in Y_{in}) with minimum principal stress (in compression) less than zero, as expressed in Eq. (10). The total number of elements under this condition is denoted as $N^{(33)}$.

$$\left(\sigma_3^{(33)} \right)_j < 0 \quad (j = 1, \dots, N_{in}) \quad (10)$$

7) Obtain the average for the minimum principal stress in compression for a vertical load case, calculated as

$$\sigma_{ave}^{(33)} = \frac{\sum_{k=1}^{N^{(33)}} \left(\sigma_3^{(33)} \right)_k}{N^{(33)}} \quad (k = 1, \dots, N^{(33)}) \quad (11)$$

where k is k th element number with the minimum principal stress in compression for a vertical load case.

8) Select the elements with lower compressive minimum principal stress than average, as written in Eq. (12), and classify them as primary trabeculae (N_{VER}). Note the above stresses have negative values. This classification process is illustrated in Fig. 3 in the box outlined by the dotted line. The above concept is based on the multiscale theory formulated in Eq. (5), which implies that under certain constant macroscopic strain, higher than average microscopic stress contributes to an increase in macroscopic stiffness. Note that this method is applicable only to human vertebral trabecular bone, which mainly supports its vertical self-weight.

$$\left(\sigma_3^{(33)} \right)_j < \sigma_{ave}^{(33)} \quad (j = 1, \dots, N_{in}) \quad (12)$$

9) Repeat steps 6 to 7 for the remaining elements in Y_{in} for the other two load cases, $\langle \sigma \rangle_{22} = -1$ and $\langle \sigma \rangle_{11} = -1$. In the same manner as that calculated in Eqs. (11) and (12), the compressive average stresses are defined. Select the elements that meet the requirements as written in either Eqs. (13) or (14), and classify them as secondary trabeculae (N_{LAT}). Note here that all load cases represent hypothetical load for the classification of vertebral trabecular bone.

$$\left(\sigma_3^{(22)} \right)_j < \sigma_{ave}^{(22)} \quad (j = 1, \dots, N_{in}) \quad (13)$$

$$\left(\sigma_3^{(11)} \right)_j < \sigma_{ave}^{(11)} \quad (j = 1, \dots, N_{in}) \quad (14)$$

10) Finally, the remaining elements in Y_{in} which are not segmented in steps 8 and 9, are then classified as no contributing trabeculae (N_{NO}). Hence, the following equation is retained with respect to the number of elements in the inner ROI.

$$N_{in} = N_{VER} + N_{LAT} + N_{NO} \quad (15)$$

Note that the classification conditions (Eqs. (12)-(14)) were applied to each voxel element. The assembly of elements is the trabeculae by visualizing them. So, if some voxel finite elements in one trabecula do not satisfy any equations (12)-(14), those elements are missing in the visualized results.

3.3 Visualization of primary bone by using dynamic FEM

Dynamic explicit FEM analysis is applied in the proposed method to enhance the visibility of the trabecular morphology. By visualizing the classified trabecular bone elements after the application of dynamic FEM under impact loading in the vertical direction, this study proposes to improve the visibility and to explain the load percolation in a complex trabecular network architecture. VOXELCON image-based FEM software (Quint Corp., Japan) was used for dynamic FEM analysis and was customized to define the element groups corresponding to the classified groups.

In the dynamic explicit FEM that uses lumped mass matrix, the numerical stability was obtained by setting the time integration that satisfies the Courants, Friedrichs, and Lewy (CFL) condition (Lewy *et al.* 1967), as shown in Eq. (16)

$$\Delta t < \frac{l}{c_v} \quad (16)$$

where Δt denotes the interval time step, l is the voxel element size, and c_v represents the velocity of the stress wave. c_v is estimated by using the following formula

$$c_v = \sqrt{\frac{E \left(\frac{1}{(1-2\nu)} + \frac{2}{(1+\nu)} \right)}{3\rho}} \quad (17)$$

where E , ν , and ρ are Young's modulus, Poisson's ratio, and the density of trabecular bone tissue, respectively.

Concerning the boundary conditions for highlighting the primary bone in human vertebral trabecular bone, the hypothetical impulse load in Eq. (18) is applied to the top surface of the ROI:

$$F(t) = -1 \text{ N for } 0 \leq t \leq 1.0 \times 10^{-5} \text{ s} \quad (18)$$

It should be noted that this very short total time is sufficient for visualizing the primary bone because the stress wave reaches the bottom surface in a very short time. The bottom surface of the ROI is fully constrained. The viscous boundary condition is applied to the side surfaces of the ROI for what is known as infinite boundary treatment (Lysmer and Kuhlemeyer 1969) because the stress wave reflection should be eliminated. Table 2 lists the values of parameters used in the present dynamic FEM analysis.

4. Results

Although the proposed classification method, shown in Fig. 3, allows for classification of the vertebral trabecular bone into primary and secondary bones, the focus of this study is primary bone.

Table 2 Values of parameters used in dynamic finite element method (FEM) analysis

Parameter	Value
Bone density, ρ (kg/mm ³)	1.94×10^{-6}
Wave velocity, c_v (mm/s)	3.3×10^6
Total time, T (s)	1.0×10^{-5}
Time step interval, Δt (s)	6.0×10^{-9}
Number of steps	1.67×10^3

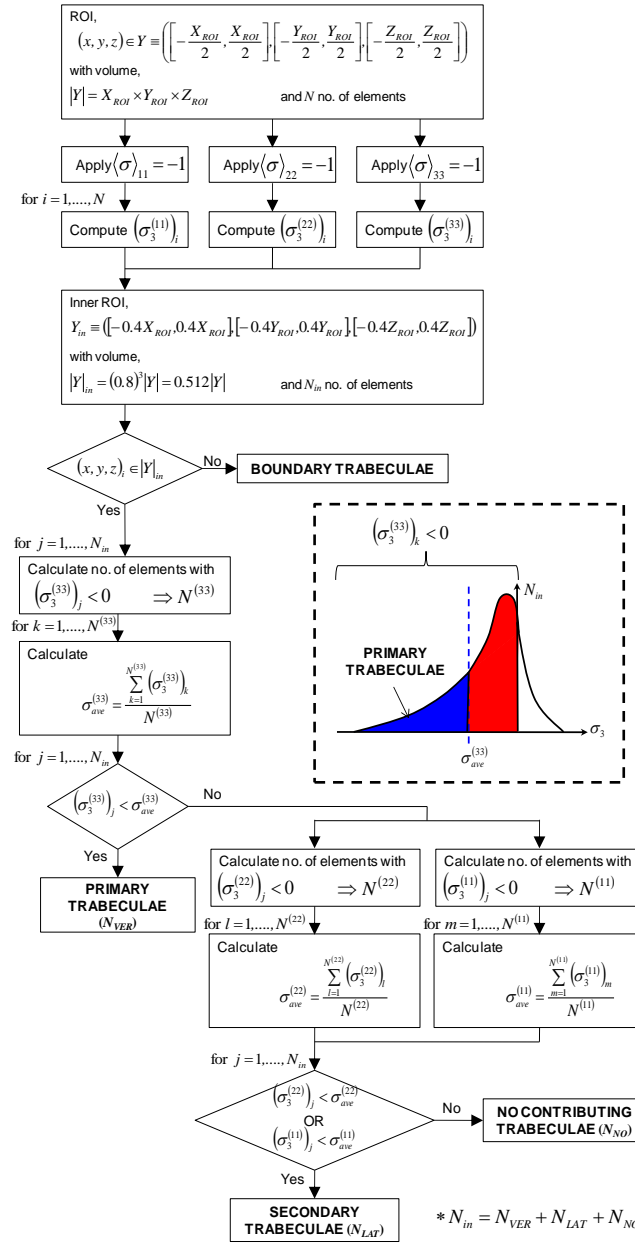


Fig. 3 Algorithm of classification procedure applied to trabecular bone.

By applying this method to the ROIs shown in Fig. 1, the classified primary trabecular bone for both osteoporotic and healthy models was extracted, as shown in Fig. 5. The primary trabecular bone appeared mainly in the vertical direction (axis-3). For osteoporotic bone, the primary trabecular bone was approximately one-third of the total volume, whereas approximately half of primary trabecular bone was extracted from the total volume of the healthy bone. Here, in comparison with the original models shown in Fig. 1, the complicated trabecular morphology was simplified and classified solely into functional bone structures against their vertical self-weight. At this point, small fragments were included in the classified primary bone group due to numerical error near the boundary region. In the following visualization step after dynamic FEM, however, only important trabeculae are highlighted.

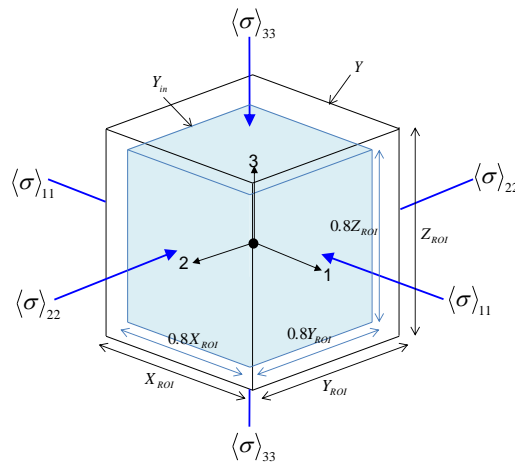


Fig. 4 Graphical definition of axes, region of interest and macroscopic stress

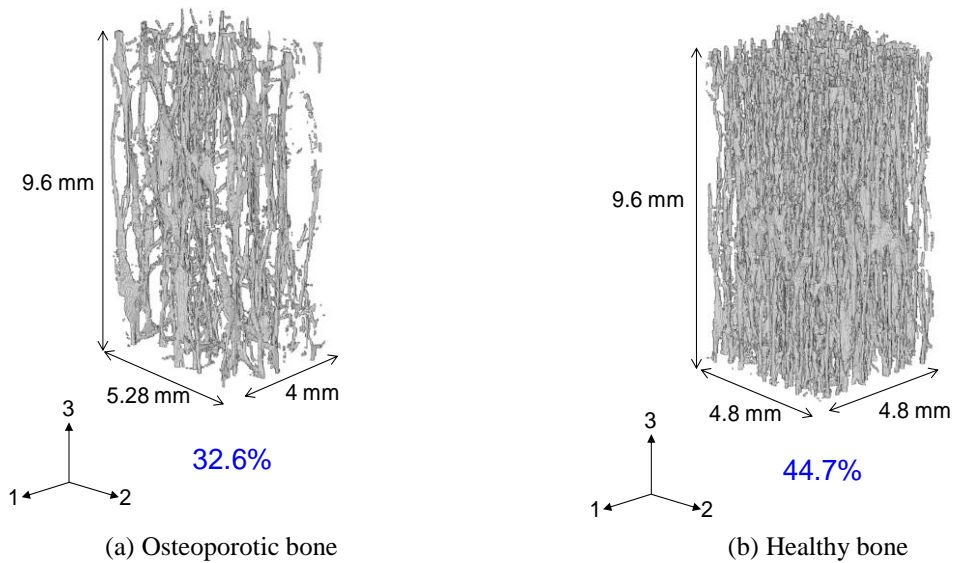


Fig. 5 Visualization of primary trabecular bone

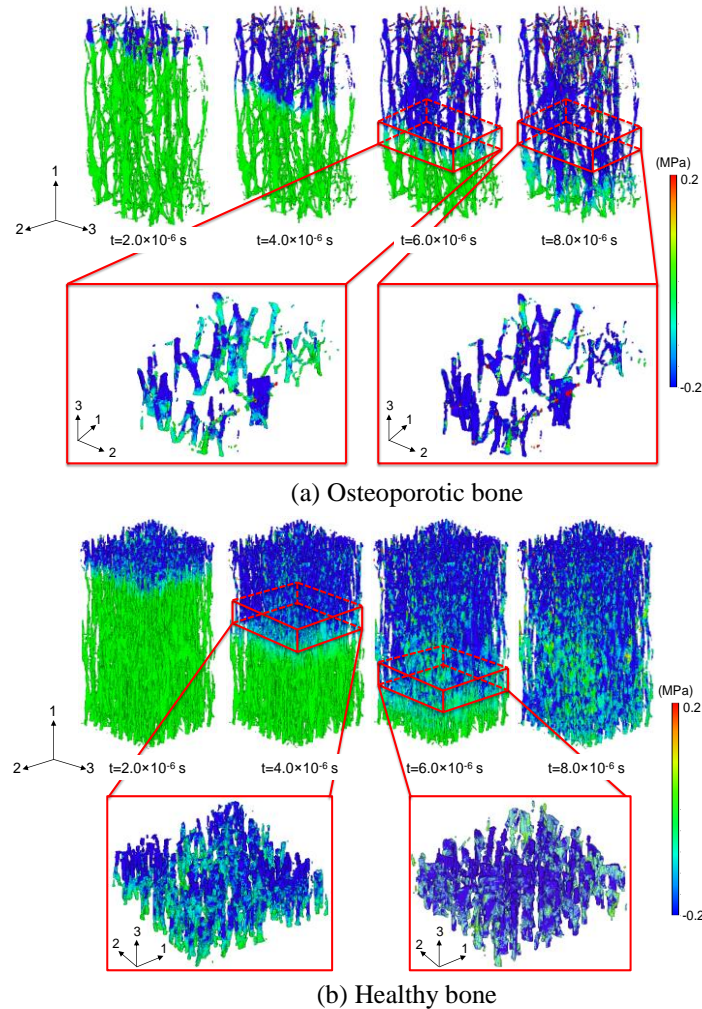


Fig. 6 Visualization of minimum principal stress distribution under impact load in selected primary trabecular bone. The contour represents the minimum principal stress distribution

The minimum principal stress distribution obtained during dynamic FEM postprocessing under compressive impact loading for the osteoporotic bone is displayed in Fig. 6(a). The blue-colored portion in the figure represents the compressive part of the minimum principal stress. Fig. 6(a) shows the stress wave propagation from top to bottom of the model in addition to the mechanically percolated trabecular bone architecture. Nearly all regions showed compression against the impact load applied to the top surface. The trabeculae were counted easily by observing the magnified view in Fig. 6(a), which also clearly shows branching at the microscale. The low bone volume fraction at 6% and the lower fraction for the primary bone at approximately 2% also contributed to the enhanced visibility.

Similarly, Fig. 6(b) shows the results for healthy bone. The volume fraction of the healthy bone was 17.2%, half of which was classified as primary bone. Figs. 5(b) and 6(b) show slight such as that shown Fig. 6(b), the trabeculae were again easily counted. Nearly all regions were in

compression, which implies successful extraction of the primary trabecular bone supporting the load and serving as a load pathway.

Note here that the stress levels (min=-0.2, max=0.2) in Fig. 6 have been adjusted consistently for both healthy and osteoporotic cases in order to put more emphasis on displaying the compressive portion of primary trabecular bone, which is in blue color. However, since the same unit macroscopic stress, $\langle \sigma \rangle_{kl}$ is applied in both cases, the osteoporotic bone with much lower stiffness, D_{pqkl}^H , might be suffered from higher strain, $(D_{pqkl}^H)^{-1} \langle \sigma \rangle_{kl}$, than the healthy bone.

5. Discussion

Trabecular morphology is influenced by the bone remodeling process, which involves the balancing activities of osteoblasts and osteoclasts. As a result of such remodeling, the bone density, or the bone volume fraction, is an important parameter used to characterize the mechanical properties of trabecular bone. In human vertebrae, two categories are also important: primary and secondary bones and plate-like and rod-like bones. The plate-like bones work as a hub in the network architecture to distribute the load to connected rod-like bones. Hence, the number of plate-like bones and connected rod-like bones can be a parameter used to explain bone quality. However, the focus of the present study is primary trabecular bone aligned in the vertical direction because the vertebral trabecular bone mainly supports its vertical self-weight.

An unexpected result of this study was such that the percentage of the primary bone for osteoporotic and healthy vertebrae in each ROI volume was lower than that in the osteoporotic bone. Although the total bone volume fraction was lower in the osteoporotic case, the decrease in primary trabecular bone was outstanding. Hence, the decrease of primary trabecular bone in osteoporotic bone reduced the bone strength in vertical direction. On the other hand, such a low number of primary trabeculae in the osteoporotic bone could be subject to stress concentration by the thinning of each trabecular strut (Blain *et al.* 2008). However, since the main purpose of this paper is to visualize the primary trabecular bone, hence the stress concentration is not displayed. Similarly, Homminga *et al.* (2004) reported that the number of overloaded trabeculae in osteoporotic vertebra is higher than that in healthy bone under normal daily loading. Visualization of primary trabecular bones, as shown in Figs. 5 and 6, could describe such phenomena. Primary trabecular bone appeared to play a key role in load-bearing capability. Therefore, an increase in primary trabecular bone would contribute to greater stiffness in the vertical direction. The secondary trabecular bone for the osteoporotic model is shown in Fig. 7. The minimum principal stress distribution is also displayed in the figure, in which the red and blue coloring indicate the trabeculae under tension and compression, respectively. All trabeculae are included in Fig. 7(a), and only the secondary trabeculae are shown in Fig. 7(b). In Fig. 7(a), compression was observed at the front part of the stress wave, and the region under tension followed. In the secondary trabecular bone, the dominant tensile part differed from that in the primary bone likely because a sufficient amount of secondary trabecular bone worked in conjunction with the primary bone in this osteoporotic case in order to ensure the effectiveness of load transfer in trabecular network. Note that the main orientation of secondary trabecular bone is in lateral direction. Hence, most of the secondary trabecular bones subject to tension under vertical compression load in order to hold the primary trabecular bone.

Moreover, the propagation of the stress wave in individual trabecula was not constant, as

shown in the magnified view in Fig. 6. In the osteoporotic case, the stress wave at $t=6\times 10^{-6}$ s reached the bottom of the magnified portion for some of the trabecular struts and fully penetrated all trabecular struts at $t=8\times 10^{-6}$ s. This difference in wave propagation occurred because the trabecular network paths were not always straight. In addition, it was supposed that the load transfer from one trabecula to another via plate-like bone influenced the wave propagation. Such difference in wave propagation for healthy case is shown in Fig. 6(b). More detailed investigation of the morphology parameters such as the number of trabeculae, the cross-section size, and force will be conducted in the future.

It is widely accepted that the load-bearing capability of each trabecular strut determines trabecular stiffness (Gefen 2009). By viewing only the percolation of the vertical load in the original trabecular structure, as shown in Fig. 7(a), it is difficult to determine the effects of trabecular struts on the mechanical load transfer. Not all of the trabecular struts in the trabecular network contribute to the load-bearing capability because orientation, connectivity, and geometry are also integral to the trabecular structure. Such less-functional trabecular struts were eliminated by the proposed classification method. By observing and measuring only the percolated network architecture, as shown in Fig. 6, the robustness and brittleness can be discussed more accurately and quantitatively, as will be presented in future research. In addition, percolation of load transfer in secondary trabecular bone for healthy bone which is not discussed in this paper due to highly complicated microarchitecture, will be also investigated further in future.

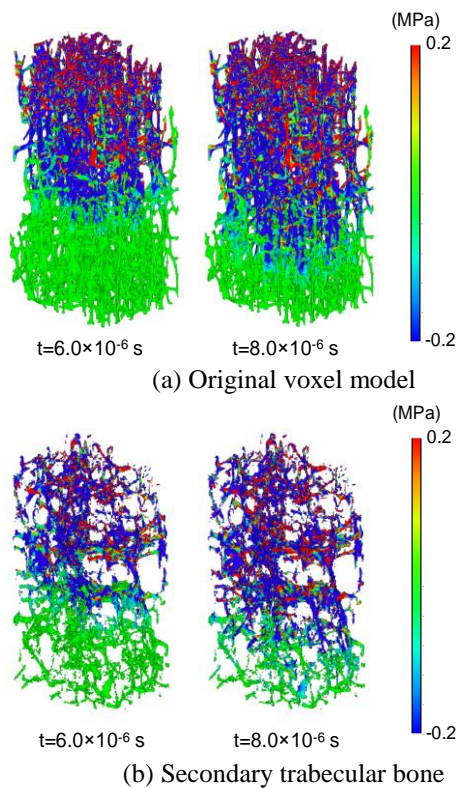


Fig. 7 Visualization of minimum principal stress distribution under impact load in selected secondary trabecular bone for osteoporotic case

6. Conclusions

In this study, a new classification method was proposed to visualize a 3D primary trabecular bone in a human L4 vertebra by using the homogenization theory. A static homogenization method was used for this classification and was combined with a dynamic explicit FEM for visualization. The proposed method allows the primary trabecular bone in a large-scale model to be extracted from a highly complicated trabecular microstructure and visualized in 3D for the first time. This research provides additional insight for investigating the role of trabecular microarchitecture in load-bearing applications, such as determination of the volumetric percentages of primary and secondary bones and stress wave propagation relative to the straightness of the primary bone. Finally, we expect that the method developed here will be extended in the future to be used for advanced morphological characterization in the quantitative estimation of brittleness.

Acknowledgments

We wish to acknowledge the contribution of Prof. Yuji Nakajima and Prof. Hiroshi Kiyama for providing the bone specimen approved by the Ethics Committee of Osaka City University. We thank Dr. Takuya Ishimoto and Dr. Sayaka Miyabe, both of Osaka University, for preparing the micro-CT images. This work was supported in part by the Ministry of Higher Education (MOHE), Malaysia, under a scholarship for the Academician Training Scheme.

References

- Andrade Silva, F., Williams, J.J., Müller, B.R., Hentschel, M.P., Portella, P.D. and Chawla, N. (2010), "Three-dimensional microstructure visualization of porosity and Fe-rich inclusions in SiC particle-reinforced Al alloy matrix composites by X-Ray synchrotron tomography", *Metall. Mater. Trans. A*, **41**(8), 2121-2128.
- Basaruddin, K.S., Takano, N., Akiyama, H. and Nakano, T. (2013), "Uncertainty modeling in the prediction of effective mechanical properties using stochastic homogenization method with application to porous trabecular bone", *Mater. Trans.*, **54**(8), 1250-1256.
- Basaruddin, K.S., Takano, N. and Nakano, T. (2013), "Stochastic multi-scale prediction on the apparent elastic moduli of trabecular bone considering uncertainties of biological apatite (BAP) crystallite orientation and image-based modeling", *Comput. Methods Biomech. Biomed. Eng.* doi: 10.1080/10255842.2013.785537.
- Blain, H., Chavassieux, P., Portero-Muzy, N., Bonnel, F., Canovas, F., Chammas, M., Maury, P. and Delmas, P.D. (2008), "Cortical and trabecular bone distribution in the femoral neck in osteoporosis and osteoarthritis", *Bone*, **43**(5), 862-868.
- Gefen, A. (2009). *Finite Element Modeling of the Microarchitecture of Cancellous Bone: Techniques and Applications (Biomechanical Systems Technology: Muscular Skeletal Systems)*, World Scientific Pub. Co. Pte. Ltd., Singapore.
- Grimal, Q., Rus, G., Parnell, W.J. and Laugier, P. (2011), "A two-parameter model of the effective elastic tensor for cortical bone", *J. Biomech.*, **44**(8), 1621-1625.
- Guedes, J. and Kikuchi, N. (1990), "Preprocessing and postprocessing for materials based on the homogenization method with adaptive finite element methods", *Comput. Methods Appl. Mech. Eng.*, **83**(2), 143-198.
- Hollister, S.J., Brennan, J.M. and Kikuchi, N. (1994), "A homogenization sampling procedure for

- calculating trabecular bone effective stiffness and tissue level stress”, *J. Biomech.*, **27** (4), 433-444.
- Hollister, S.J., Fyhrie, D.P., Jepsen, K.J. and Goldstein, S.A. (1991) “Application of homogenization theory to the study of trabecular bone mechanics”, *J. Biomech.*, **24**(9), 825-839.
- Homminga, J., Van-Rietbergen, B., Lochmüller, E.M., Weinans, H., Eckstein, F. and Huiskes, R. (2004), “The osteoporotic vertebral structure is well adapted to the loads of daily life, but not to infrequent “error” loads”, *Bone*, **34**(3), 510-516.
- Keyak, J.H., Meagher, J.M., Skinner, H.B. and Mote, Jr. C.D. (1990), “Automated three-dimensional finite element modelling of bone: A new method”, *J. Biomed. Eng.*, **12**(5), 389-397.
- Kinney, J.H. and Ladd, A.J.C. (1998), “The relationship between three-dimensional connectivity and the elastic properties of trabecular bone”, *J. Bone Miner. Res.*, **13**(5), 839-845.
- Kuhlemeyer, R.L. and Lysmer, J. (1973), “Finite element method accuracy for wave propagation problems”, *J. Soil Mech. Found. Div., Proc. Am. Soc. Civil Eng.*, **99**(5), 421-427.
- Lee, S.G., Gokhale, A.M. and Sreeranganathan, A. (2006), “Reconstruction and visualization of complex 3D pore morphologies in a high-pressure die-cast magnesium alloy”, *Mater. Sci. Eng.: A*, **427**(1), 92-98.
- Lewy, H., Friedrichs, K. and Courant, R. (1967), “On the partial difference equations of mathematical physics”, *IBM J. Res. Dev.*, **11**(2), 215-234.
- Lin, C. and Cohen, M.H. (1982), “Quantitative methods for microgeometric modeling”, *J. Appl. Phys.*, **53**(6), 4152-4165.
- Liu, X.S., Bevill, G., Keaveny, T.M., Sajda, P. and Guo, X.E. (2009), “Micromechanical analyses of vertebral trabecular bone based on individual trabeculae segmentation of plates and rods”, *J. Biomech.*, **42**(3), 249-256.
- Liu, X.S., Sajda, P., Saha, P.K., Wehrli, F.W., Bevill, G., Keaveny, T.M. and Guo, X.E. (2008), “Complete volumetric decomposition of individual trabecular plates and rods and its morphological correlations with anisotropic elastic moduli in human trabecular bone”, *J. Bone Miner. Res.*, **23**(2), 223-235.
- Lysmer, J. and Kuhlemeyer, R.L. (1969), “Finite dynamic model for infinite media”, *J. Eng. Mech. Div., Proc. Am. Soc. Civil Eng.*, **95**(4), 859-877.
- Matsunaga, S., Naito, H., Tamatsu, Y., Takano, N., Abe, S. and Ide, Y. (2013), “Consideration of shear modulus in biomechanical analysis of peri-implant jaw bone: Accuracy verification using image-based multi-scale simulation”, *Dental Mater. J.*, **32**(3), 425-432.
- Nakano, T., Kaibara, K., Tabata, Y., Nagata, N., Enomoto, S., Marukawa, E. and Umakoshi, Y. (2002), “Unique alignment and texture of biological apatite crystallites in typical calcified tissues analyzed by microbeam x-ray diffractometer system”, *Bone*, **31**(4), 479-487.
- Ohashi, T., Matsunaga, S., Nakahara, K., Abe, S., Ide, Y., Tamatsu, Y. and Takano, N. (2010), “Biomechanical role of peri-implant trabecular structures during vertical loading”, *Clin. Oral Investig.*, **14**(5), 507-513.
- Parnell, W.J., Grimal, Q., Abrahams, I.D. and Laugier, P. (2006), “Modelling cortical bone using the method of asymptotic homogenization”, *J. Biomech.*, **39**(1), S20.
- Pothuaud, L., Porion, P., Lespessailles, E., Benhamou, C.L. and Levitz, P. (2000), “A new method for three-dimensional skeleton graph analysis of porous media: application to trabecular bone microarchitecture”, *J. Microscopy*, **199**(2), 149-161.
- Reilly, D.T. and Burstein, A.H. (1975), “The elastic and ultimate properties of compact bone tissue”, *J. Biomech.*, **8**(6), 393-405.
- Rho, J.Y., Ashman, R.B. and Turner, C.H. (1993), “Young’s modulus of trabecular and cortical bone material: Ultrasonic and microtensile measurements”, *J. Biomech.*, **26**(2), 111-119.
- Saha, P.K., Gomberg, B.R. and Wehrli, F.W. (2000), “Three-dimensional digital topological characterization of cancellous bone architecture”, *Int. J. Imaging Syst. Technol.*, **11**(1), 81-90.
- Shi, X., Wang, X. and Niebur, G.L. (2009), “Effects of loading orientation on the morphology of the predicted yielded regions in trabecular bone”, *Ann. Biomed. Eng.*, **37**(2), 354-362.
- Stauber, M. and Müller, R. (2006), “Volumetric spatial decomposition of trabecular bone into rods and plates-A new method for local bone morphometry”, *Bone*, **38**(4), 475-84.
- Takano, N., Fukasawa, K. and Nishiyabu, K. (2010), “Structural strength prediction for porous titanium

- based on micro-stress concentration by micro-CT image-based multiscale simulation”, *Int. J. Mech. Sci.*, **52**(2), 229-235.
- Takano, N., Zako, M., Kubo, F. and Kimura, K. (2003), “Microstructure-based stress analysis and evaluation for porous ceramics by homogenization method with digital image-based modeling”, *Int. J. Solid. Struct.*, **40**(5), 1225-1242.
- Tawara, D., Adachi, T., Takano, N., Nakano, T., Umakoshi, Y., Kobayashi, A., Iwaki, H. and Takaoka, K. (2008), “High-resolution micro-mechanical analysis of cancellous bone in vertebra considering bone quality”, *Jpn. J. Clin. Biomech.*, **29**, 7-14. (in Japanese)
- Tawara, D., Takano, N., Adachi, T. and Nakano, T. (2010), “Mechanical evaluation of trabecular bone of human vertebra based on multi-scale stress analysis”, *J. Jpn. Soc. Bone Morphom.*, **20**, S100-S107. (in Japanese)
- Van Buskirk, W.C. and Ashman, R.B. (1981), “The elastic moduli of bone”, *Tran. Am. Soc. Mech. Eng. (Appl. Mech. Div.)*, **45**, 131-143.

TA